Giant enhancement in the ferroelectric field effect using a polarization gradient

Zongquan Gu,[1] Mohammad A. Islam,[2,3] and Jonathan E. Spanier[1,2,4,a)]
[1]Department of Electrical and Computer Engineering, Drexel University, Philadelphia, Pennsylvania 19104, USA
[2]Department of Materials Science and Engineering, Drexel University, Philadelphia, Pennsylvania 19104, USA
[3]Department of Physics, State University of New York at Oswego, Oswego, New York 13126, USA
[4]Department of Physics, Drexel University, Philadelphia, Pennsylvania 19104, USA

(Received 24 August 2015; accepted 30 September 2015; published online 19 October 2015)

Coupling of switchable ferroelectric polarization with the carrier transport in an adjacent semiconductor enables a robust, non-volatile manipulation of the conductance in a host of low-dimensional systems, including the two-dimensional electron liquid that forms at the $LaAlO_3$ (LAO)-$SrTiO_3$ (STO) interface. However, strength of the gate-channel coupling is relatively weak, limited in part by the electrostatic potential difference across a ferroelectric gate. Here, through application of phenomenological Landau-Ginzburg-Devonshire theory and self-consistent Poisson-Schrödinger model calculations, we show how compositional grading of $PbZr_{1-x}Ti_xO_3$ ferroelectric gates enables a more than twenty-five-fold increase in the LAO/STO channel conductance on/off ratios. Incorporation of polarization gradients in ferroelectric gates can enable breakthrough performance of ferroelectric non-volatile memories. © *2015 AIP Publishing LLC*. [http://dx.doi.org/10.1063/1.4933095]

The ferroelectric field-effect transistor (FET) is promising for non-volatile memory elements and other functionalities associated with incorporation of switchable polarization.[1–3] Large figures of merit, i.e., ratios of drain and source currents or of resistances in the on and off states, have been reported in ferroelectrically gated two- or one-dimensional channels, e.g., $Pb(Zr,Ti)O_3$ with MoS_2,[4] graphene,[5] carbon nanotubes,[6] and ZnO nanowires.[7] The effect has also been demonstrated using organic ferroelectric polyvinylidene fluoride (PVDF) on various channels,[8,9] $LiNbO_3$ with MoS_2,[3] $BaTiO_3$ with carbon nanotubes,[10] and the relaxor ferroelectric $Pb(Mn,Nb)O_3$-$PbTiO_3$ (PMN-PT) with graphene.[11] Compared with ferroelectric random access memories, ferroelectric field-effect memories are more scalable and consume less power since there is no requirement for charge amplification and transistor-capacitor architecture.[12]

The discovery[13] of a two dimensional electron liquid (2DEL) at the interface of $LaAlO_3$ (LAO) and $SrTiO_3$ (STO) has been followed by observation of remarkable properties at this interface.[14–17] The similar interfacial conductivities in other STO-based oxide heterostructures[18–20] have stimulated the development of prototype FETs.[21,22] However, the poor interface between oxides and common metal electrodes can deteriorate device properties.[23,24] While local surface control of 2DEL enables nanoscale reconfigurable electronics, these devices retain their written state only on the timescale of hours.[25,26]

Recently, ferroelectric polarization in a $Pb(Zr_{0.2}Ti_{0.8})O_3$ (PZT) gate[2,27] on LAO/STO has been shown to be an isostructural all-oxide route for non-volatile manipulation of the near-surface 2DEL. Orientation of the out-of-plane polarization P_3 in the PZT layer was found to couple directly to the Sr 3*d* core level and to depletion and accumulation of the electrons at the interface.[2] Therefore, the field-effect is largely dependent on the ferroelectric properties of the film, particularly the size of the potential drop across the film V_{PZT}, which is nearly zero in cases of almost complete screening of polarization charge.

Introduction of gradients in the composition and/or strain in ferroelectric thin films, producing gradients in ferroelectric polarization and in electrostatic potential, can be highly effective in achieving significant improvements in the dielectric, pyroelectric, and piezoelectric properties[28–32] with device implications,[33] where the graded PZT films have been grown by pulsed laser deposition (PLD),[31,32] sputtering,[34] and metalorganic chemical vapor deposition (MOCVD).[35] Here we show, using calculations coupling Landau-Ginzburg-Devonshire (LGD) theory in $PbZr_{1-x}Ti_xO_3$ with self-consistent Poisson-Schrödinger (PS) models in adjacent LAO-STO channel, how design and incorporation of a polarization gradient across the film thickness enables an increase in the gating ratio of more than 2500% compared with the gradient-free case for the same film thickness.

We consider a PZT ferroelectric gate on an LAO/STO 2DEL. We incorporate the ferroelectric properties of the PZT gate by V_{PZT} within the PS model to study its effect on the spatially modulated volume electron density n_e at and near the LAO/STO interface, and then calculate the conductivity σ. V_{PZT} is induced by the spatial variation of P_3 as determined in the LGD model. The ferroelectric free energy $G_{tot} = \int_0^L (g_{bulk} + g_{grad} + g_{dep} + g_{flexo})\, dx_3$, where g_{bulk}, g_{grad}, g_{dep}, and g_{flexo} are the bulk, gradient, depolarization, and flexoelectric energy densities, and L is the PZT film thickness. Minimizing G_{tot} yields the P_3 master equation (see supplementary material[36]). Since the PS solution (see supplementary material[36]) accounts for overlapping of the electrostatic potential build-up in LAO and band bending in STO, incorporation of the PZT ferroelectricity is introduced through its electrostatic (field-effect) doping on the system.

[a)]Email: spanier@drexel.edu

Reuse of AIP Publishing content is subject to the terms at: https://publishing.aip.org/authors/rights-and-permissions. IP: 144.118.64.216 On: Tue, 01 Mar 2016 11:09:11

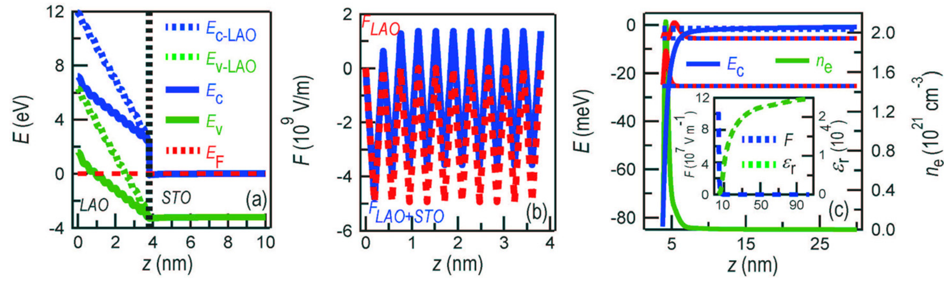

FIG. 1. (a) Band profile of a 10 u.c. LAO on STO at $T = 4.2$ K. The blue and green dashes show the intrinsic potential in LAO. The black dashes are LAO-STO boundary, and red dashes are Fermi level. (b) The electric field F in LAO for both cases in (a). (c) The band bending formed in STO with its subbands, the square magnitude of the eigenwaves at the 1st and 2nd levels and n_e. The inset shows F and ε_r in STO.

In our model, the overlapping between the LAO valence band maximum (VBM) and the STO conduction band minimum (CBM) is decreased (increased) when PZT is polarized up (down), and in both cases, the modulation magnitude is equal to V_{PZT}.

The self-consistent PS method has been employed to model the III-V,[37] III-N,[38] and STO-based heterostructures.[39,40] But understanding the discrepancy in electron sheet density n_{ss} between experiment and theory, and n_{ss} dependence on temperature T remains lacking. Incorporating an orbital-resolved effective electron mass m_e and T, we find quantitative agreement of n_{ss} with experiment and theory and reveal its independence with T. For a 10 unit cell (u.c.) LAO on STO at $T = 4.2$ K (Fig. 1(a)), we find a 1.67 eV overlap between the LAO VBM and the STO CBM compared with an intrinsic 6.8 eV potential build-up in LAO. The potential drop indicates the electron transfer from the LAO surface to the interface, forming a sheet of electrons $n_{ss} = 1.81 \times 10^{14}\,\text{cm}^{-2}$ and leaving an identical number of holes in LAO to maintain charge neutrality. As a result, the electric field F becomes positive in a portion of the LAO (Fig. 1(b)), making the LAO potential increase or decrease depending on the polarity of F rather than linearly rise when F is non-positive before the electron transfer. The transferred electrons form an 80 meV band bending in STO (Fig. 1(c)) where the Fermi level E_F is at -1 meV. There are 1 hole and 4 electron subbands populated above and under E_F, respectively, and their wave extensions are longer than the Fermi wavelength. The electrons are distributed within 3.5 nm where n_e decays to 1% of its peak value in STO. Consequently, F rapidly decreases to zero from the interface, as does its modulation on the permittivity ε_r (inset).

Electron localization is ascribed to a heavy d_{xz}-orbital $m_e = 14m_0$[41] at low T. Calculations with different m_e and T were conducted to determine the effect of each. In Fig. 2(a), using identical m_e, the band bending increases for temperatures up to $T = 65$ K above which ε_r becomes independent of F[42] and as a result, the integrated F and band bendings in the Poisson equation become lower. Above $T = 65$ K, the band bending again increases, to 260 meV at 300 K, to counteract the thermal activation of the electrons. However, n_{ss} remains $\sim 1.83 \times 10^{14}\,\text{cm}^{-2}$ and the electrons are still confined within several nanometers in all T. Next, the band bending with different m_e at $T = 300$ K are calculated (Fig. 2(b)). An orbital-resolved m_e is employed at the heavy and light m_e regions,[43] respectively. First, we assign m_e to a d_{yz}-orbital $0.7m_0$[41] and

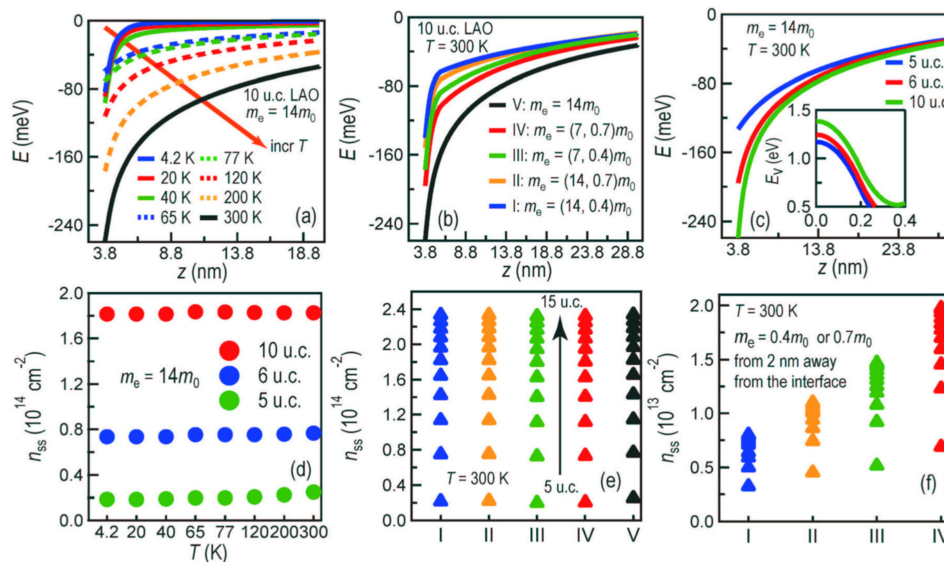

FIG. 2. Band bendings of 10 u.c. LAO for (a) $m_e = 14m_0$ and various T, and (b) $T = 300$ K and various m_e. We define the heavy m_e region from the interface to 2 nm away and the light afterwards. The values of m_e in the two regions in I, II, III, IV are shown in the inset. (c) The comparison of 5, 6, and 10 u.c. LAO at $m_e = 14m_0$ and $T = 300$ K and the LAO VBMs shown in the inset. (d) The total n_{ss} of 5, 6, and 10 u.c. LAO with $m_e = 14m_0$ at different T. (e) n_{ss} in total and (f) n_{ss} in the light m_e region at $T = 300$ K of 5–15 u.c. LAO for m_e in I, II, III, IV, and V in (b). These results show that the total n_{ss} approaches the theoretical value $3.3 \times 10^{14}\,\text{cm}^{-2}$ over a wide T and m_e range and n_{ss} in the light m_e region yields quantitative agreement with experiment which is usually an order of magnitude lower.

Reuse of AIP Publishing content is subject to the terms at: https://publishing.aip.org/authors/rights-and-permissions. IP: 144.118.64.216 On: Tue, 01 Mar 2016 11:09:11

$0.4m_0$[44] from 2 nm away from the interface for the light m_e region. The band bending decreases to about 150 meV and 140 meV, respectively, because F, whose first derivative in the Poisson equation has a linear dependence on m_e in n_e, is suppressed in the light m_e region and henceforth the band bending. Then, m_e is changed from $14m_0$ to $7m_0$[45] from the interface to 2 nm away in the heavy m_e region for both cases and the band bending increases to about 200 meV and 178 meV, respectively, restricting the escape of electrons due to the decrease in m_e. Compared with the constant m_e, the slopes in the heavy m_e region are much steeper than the light m_e in response to the sharp m_e contrast, but n_{ss} remains $\sim 1.8 \times 10^{14}\,\mathrm{cm}^{-2}$ in each case.

Though m_e and T have a profound impact on the band bending, n_{ss} and the electron localization are preserved because of the intrinsic potential build-up in LAO, verified by the comparisons of 5 and 6 u.c. LAO at $m_e = 14m_0$ and $T = 300\,\mathrm{K}$ (Fig. 2(c)). The band bending reduces with the LAO u.c. because of less overlap of the LAO VBM with the LAO VBM and the STO CBM shown in the inset, leading to $n_{ss} = 2.5 \times 10^{13}\,\mathrm{cm}^{-2}$ and $7.7 \times 10^{13}\,\mathrm{cm}^{-2}$. The effect of T and m_e on n_{ss} is shown in Figs. 2(d) and 2(e), where n_{ss} stays unchanged over a wide range of T and in all orbital-resolved m_e cases, and n_{ss} increases from $2.5 \times 10^{13}\,\mathrm{cm}^{-2}$ for 5 u.c., to $2.3 \times 10^{14}\,\mathrm{cm}^{-2}$ for 15 u.c., approaching the theoretical value.[13] The discrepancy between the calculated and experimental n_{ss} could be addressed by counting n_{ss} with orbital-resolved m_e shown in Fig. 2(f). n_{ss} in the light m_e region from I to IV in Fig. 2(b) increases from $6.9 \times 10^{12}\,\mathrm{cm}^{-2}$ for 5 u.c. to $2.0 \times 10^{13}\,\mathrm{cm}^{-2}$ for 15 u.c.[46] Also, the ratio between n_{ss} in the light m_e region and the total increases as the difference between heavy and light m_e is reduced.

Using values of m_e obtained from advanced experimental spectroscopies[41] and density functional theory (DFT),[43–45] the PS solution can be used to model and explain the band bending and n_{ss} over a wide range of T, yielding quantitative agreement with theoretical and experiment values. Though the heavy-m_e electrons occupies a large fraction in the total, their contribution to the conductivity σ is inhibited by the much lower mobility μ (supplementary material[36]).

Polarization profiles of $\mathrm{PZT}_{0.8}$ films with different gradient energy coefficient g_{33}, extrapolation length δ and L are shown in Fig. 3(b). Spontaneous P_3 with $\delta = \infty$ is 68 $\mu\mathrm{C/cm}^2$. For a realistic value of δ (=1.9 nm),[47] P_3 decreases near the surface and interface, and maintains uniformity in the middle. The P_3 profile is dependent on g_{33} and L. For example, for a 50 nm-thick film, V_{PZT} increases from 22 meV to 67 meV when g_{33} changes from $3.46 \times 10^{-10}\,\mathrm{m}^2\,\mathrm{J}\,\mathrm{C}^{-2}$ to $3.46 \times 10^{-9}\,\mathrm{m}^3\,\mathrm{J}\,\mathrm{C}^{-2}$ and saturates at 71 meV when $L = 150\,\mathrm{nm}$ or thicker. However, it drops to 31 meV when δ increases from 1.9 nm to 5 nm (Fig. 3(c)). Since g_{33} and δ are largely dependent on the as-grown property of the film, V_{PZT} in a single-composition film is limited by thickness and varies extensively with growth conditions. These two shortages suppress the modulation effect, and we propose they can be overcome by a compositionally graded film,[31,32,48] where V_{PZT} is dependent on the composition gradient and increases with thickness. The P_3 of a graded film whose composition smoothly varies from $\mathrm{PZT}_{0.2}$ to $\mathrm{PZT}_{0.8}$ is shown in Fig. 3(e). Unlike the single-composition, P_3 in the middle varies with composition, and hence, V_{PZT} is dominated by the potential drops in the interior through the relatively large L/δ ratio (Fig. 3(f)). V_{PZT} increases to 192 meV and 212 meV for a 50 nm film with different pairs of values of g_{33}, 3–8 times larger than that for single-composition $\mathrm{PZT}_{0.8}$, and it continues to increase, to 372 meV for $L = 100\,\mathrm{nm}$, regardless of δ. The weak dependence of V_{PZT} on g_{33} and on δ, combined with its steady increase with L, makes the graded film a better choice over the single composition.

The doping effect of a 50 nm-thick graded PZT layer on a 5 u.c. LAO/STO with heavy $m_e = 7m_0$ and light $0.7m_0$ at $T = 300\,\mathrm{K}$ is shown in Fig. 4(a). The modified band bandings and the LAO VBMs in the inset are 32 meV and 1.13 eV, respectively, for upward P_3, and 112 meV and 1.44 eV, respectively, for downward P_3. Compared with the intrinsic values (77 meV and 1.28 eV), the LAO and STO overlapping is tuned to be 192 meV shallower and deeper to balance V_{PZT} in each case. n_{ss} in the heavy and light m_e regions are $4.1 \times 10^{13}\,\mathrm{cm}^{-2}$ and $1.1 \times 10^{13}\,\mathrm{cm}^{-2}$, respectively, for downward P_3, and $2 \times 10^{12}\,\mathrm{cm}^{-2}$ and $1.2 \times 10^{12}\,\mathrm{cm}^{-2}$, respectively, for upward P_3. The doping increment is diminished by the increasing LAO thickness (Fig. 4(b)) where it is seen that a thinner LAO is always desired to achieve a better doping effect. We investigate the doping effect as a function of the graded PZT thickness on a 5 u.c. LAO: the splitting of n_{ss} between upward and downward P_3 in both the heavy and

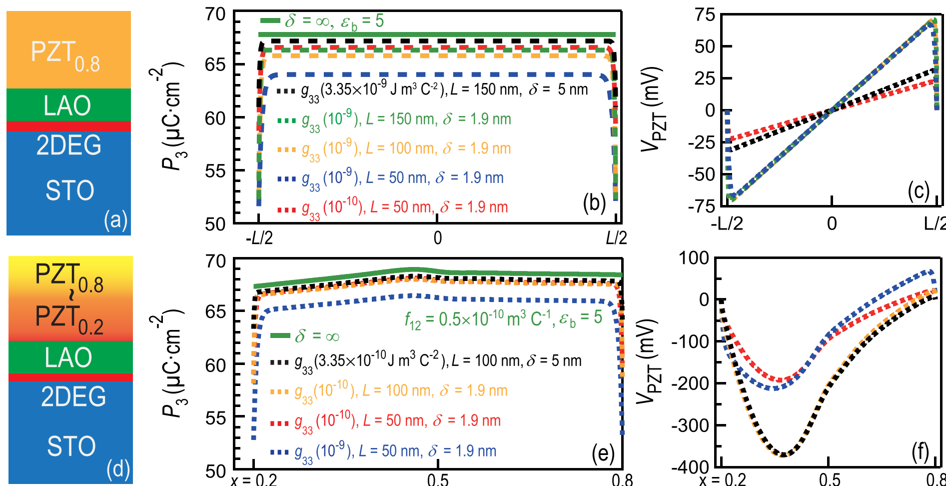

FIG. 3. P_3 profiles of a single-composition $\mathrm{PZT}_{0.8}$ film (b) and a graded $\mathrm{PZT}_{0.2} \sim \mathrm{PZT}_{0.8}$ film (e) shown in (a) and (d). The corresponding potential variations V_{PZT} are shown in (c) and (f) where the line types are denoted in the legend for (b) and (e), respectively.

Reuse of AIP Publishing content is subject to the terms at: https://publishing.aip.org/authors/rights-and-permissions. IP: 144.118.64.216 On: Tue, 01 Mar 2016 11:09:11

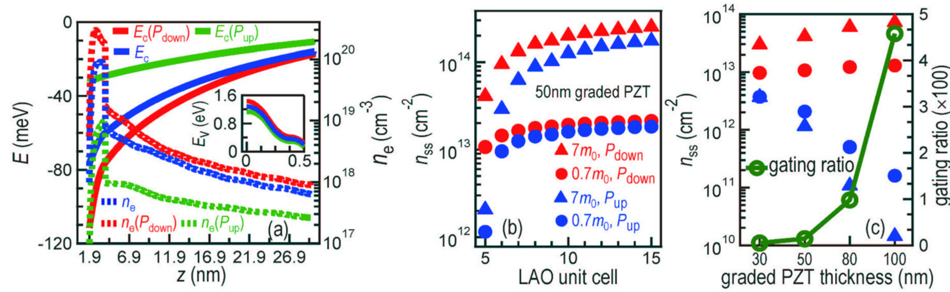

FIG. 4. (a) The band bending and n_e in a 5 u.c. LAO ($m_e = 7$ and $0.7m_0$) at $T = 300$ K modulated by a 50 nm graded PZT layer. The inset shows the corresponding LAO VBMs. (b) n_{ss} corresponding to the heavy and light m_e regions. (c) n_{ss} in the heavy and light m_e regions and the gating ratio of 5 u.c LAO with different PZT thickness where the markers are denoted by the legend in (b).

light m_e region is enhanced with the thickness L (Fig. 4(c)). The conductivity $\sigma = q\mu n_e$ is a summation in both the heavy and light m_e region where a weighting factor $n_e/\sum n_e$ is imposed at each n_e and the gating ratio, defined as the ratio of σ between P_3 down and up is increasingly steeper, reaching ~500 for a 100 nm-graded film. Though the gating ratio varies orders of magnitude depending on individual experimental conditions,[2,27] our calculation shows semi-quantitative agreement with the existing experiment.[27] As long as the smooth transition in PZT composition can be realized in thicker graded films, V_{PZT} can be enhanced with smoother P_3 gradient and stronger field-effect on the overlapping between LAO and STO, and the gating ratio can be expected.

Though the graded film provides a better field-effect than the non-graded case, the asymmetrical V_{PZT} requires higher switching field, and special attention should be paid to the strain conservation for thicker film where low Ti-ratio PZT film has large lattice mismatching with LAO-STO. Incorporation of ferroelectric polarization gradients in a non-volatile gate insulator enables significantly enhanced gate-channel coupling, manifested as a 1–2 orders of magnitude increase in the on/off ratio. While we demonstrate this for PZT/LAO/STO, ferroelectric polarization gradient-enhanced gate insulators can be introduced and coupled to other aforementioned low-dimensional channels to produce similarly large enhancements.

We acknowledge fruitful discussions with Dr. Philip D. C. King, Dr. Johan Biscaras, and Dr. Ye Cao. Numerical simulations were carried out on hardware supported by Drexel's University Research Computing Facility. Work supported by the National Science Foundation (NSF) under Award No. DMR 1124696 and the Nanoscale Research Initiative (NRI) of the Semiconductor Research Corporation (SRC) under the Nanoelectronics and Beyond in 2020 (NEB2020) Program.

[1]S. Mathews, Science **276**, 238 (1997).
[2]V. T. Tra, J. W. Chen, P. C. Huang, B. C. Huang, Y. Cao, C. H. Yeh, H. J. Liu, E. a. Eliseev, A. N. Morozovska, J. Y. Lin *et al.*, Adv. Mater. **25**, 3357 (2013).
[3]A. Nguyen, P. Sharma, T. Scott, E. Preciado, V. Klee, D. Sun, I.-H. D. Lu, D. Barroso, S. Kim, V. Y. Shur, *et al.*, Nano Lett. **15**, 3364 (2015).
[4]C. Zhou, X. Wang, S. Raju, Z. Lin, D. Villaroman, B. Huang, H. L.-W. Chan, M. Chan, and Y. Chai, Nanoscale **7**, 8695 (2015).
[5]C. Baeumer, S. P. Rogers, R. Xu, L. W. Martin, and M. Shim, Nano Lett. **13**, 1693 (2013).
[6]T. Sakurai, T. Yoshimura, S. Akita, N. Fujimura, and Y. Nakayama, Jpn. J. Appl. Phys., Part 2 **45**, L1036 (2006).
[7]L. Liao, H. J. Fan, B. Yan, Z. Zhang, L. L. Chen, B. S. Li, G. Z. Xing, Z. X. Shen, T. Wu, X. W. Sun *et al.*, ACS Nano **3**, 700 (2009).
[8]Y. Zheng, G.-X. Ni, C.-T. Toh, C.-Y. Tan, K. Yao, and B. Özyilmaz, Phys. Rev. Lett. **105**, 166602 (2010).
[9]J. Y. Son, S. Ryu, Y.-C. Park, Y.-T. Lim, Y.-S. Shin, Y.-H. Shin, and H. M. Jang, ACS Nano **4**, 7315 (2010).
[10]W. Fu, Z. Xu, X. Bai, C. Gu, and E. Wang, Nano Lett. **9**, 921 (2009).
[11]W. Jie, Y. Y. Hui, N. Y. Chan, Y. Zhang, S. P. Lau, and J. Hao, J. Phys. Chem. C **117**, 13747 (2013).
[12]N. Setter, D. Damjanovic, L. Eng, G. Fox, S. Gevorgian, S. Hong, A. Kingon, H. Kohlstedt, N. Y. Park, G. B. Stephenson *et al.*, J. Appl. Phys. **100**, 051606 (2006).
[13]A. Ohtomo and H. Y. Hwang, Nature **427**, 423 (2004).
[14]A. Brinkman, M. Huijben, M. van Zalk, J. Huijben, U. Zeitler, J. C. Maan, W. G. van der Wiel, G. Rijnders, D. H. A. Blank, and H. Hilgenkamp, Nat. Mater. **6**, 493 (2007).
[15]N. Reyren, S. Thiel, A. D. Caviglia, L. F. Kourkoutis, G. Hammerl, C. Richter, C. W. Schneider, T. Kopp, A.-S. Rüetschi, D. Jaccard *et al.*, Science **317**, 1196 (2007).
[16]C. W. Bark, P. Sharma, Y. Wang, S. H. Baek, S. Lee, S. Ryu, C. M. Folkman, T. R. Paudel, A. Kumar, S. V. Kalinin *et al.*, Nano Lett. **12**, 1765 (2012).
[17]A. Tebano, E. Fabbri, D. Pergolesi, G. Balestrino, and E. Traversa, ACS Nano **6**, 1278 (2012).
[18]W. Meevasana, P. D. C. King, R. H. He, S.-K. Mo, M. Hashimoto, A. Tamai, P. Songsiririthigul, F. Baumberger, and Z.-X. Shen, Nat. Mater. **10**, 114 (2011).
[19]H. W. Jang, D. A. Felker, C. W. Bark, Y. Wang, M. K. Niranjan, C. T. Nelson, Y. Zhang, D. Su, C. M. Folkman, S. H. Baek *et al.*, Science **331**, 886 (2011).
[20]J. Biscaras, S. Hurand, C. Feuillet-Palma, A. Rastogi, R. C. Budhani, N. Reyren, E. Lesne, J. Lesueur, and N. Bergeal, Sci. Rep. **4**, 6788 (2014).
[21]M. Boucherit, O. F. Shoron, T. A. Cain, C. A. Jackson, S. Stemmer, and S. Rajan, Appl. Phys. Lett. **102**, 242909 (2013).
[22]M. Hosoda, Y. Hikita, H. Y. Hwang, and C. Bell, Appl. Phys. Lett. **103**, 103507 (2013); e-print arXiv:1306.4351v1.
[23]S. K. Kim, S.-I. Kim, H. Lim, D. S. Jeong, B. Kwon, S.-H. Baek, and J.-S. Kim, Sci. Rep. **5**, 8023 (2015).
[24]J. Karthik, A. R. Damodaran, and L. W. Martin, Adv. Mater. **24**, 1610 (2012).
[25]F. Bi, D. F. Bogorin, C. Cen, C. W. Bark, J.-W. Park, C.-B. Eom, and J. Levy, Appl. Phys. Lett. **97**, 173110 (2010).
[26]Y. Xie, C. Bell, Y. Hikita, and H. Y. Hwang, Adv. Mater. **23**, 1744 (2011).
[27]S. I. Kim, D. H. Kim, Y. Kim, S. Y. Moon, M. G. Kang, J. K. Choi, H. W. Jang, S. K. Kim, J. W. Choi, S. J. Yoon *et al.*, Adv. Mater. **25**, 4612 (2013).
[28]J. V. Mantese, N. W. Schubring, A. L. Micheli, and A. B. Catalan, Appl. Phys. Lett. **67**, 721 (1995).
[29]Z.-G. Ban, S. P. Alpay, and J. V. Mantese, Phys. Rev. B **67**, 184104 (2003).
[30]M. B. Okatan, A. L. Roytburd, V. Nagarajan, and S. P. Alpay, J. Phys. Condens. Matter **24**, 024215 (2012).
[31]J. Karthik, R. V. K. Mangalam, J. C. Agar, and L. W. Martin, Phys. Rev. B **87**, 024111 (2013).
[32]R. V. K. Mangalam, J. Karthik, A. R. Damodaran, J. C. Agar, and L. W. Martin, Adv. Mater. **25**, 1761 (2013).

Reuse of AIP Publishing content is subject to the terms at: https://publishing.aip.org/authors/rights-and-permissions. IP: 144.118.64.216 On: Tue, 01 Mar 2016 11:09:11

[33]I. Misirlioglu, C. Sen, M. Kesim, and S. Alpay, J. Mater. Sci. 1–12 (2015).
[34]C. Wang, Q. F. Fang, Z. G. Zhu, A. Q. Jiang, S. Y. Wang, B. L. Cheng, and Z. H. Chen, Appl. Phys. Lett. **82**, 2880 (2003).
[35]C. M. Foster, G.-R. Bai, R. Csencsits, J. Vetrone, R. Jammy, L. A. Wills, E. Carr, and J. Amano, J. Appl. Phys. **81**, 2349 (1997).
[36]See supplementary material at http://dx.doi.org/10.1063/1.4933095 for the detailed derivations.
[37]I.-H. Tan, G. L. Snider, L. D. Chang, and E. L. Hu, J. Appl. Phys. **68**, 4071 (1990).
[38]P. D. C. King, T. D. Veal, and C. F. McConville, Phys. Rev. B **77**, 125305 (2008).
[39]J. Biscaras, N. Bergeal, S. Hurand, C. Grossetête, A. Rastogi, R. C. Budhani, D. Leboeuf, C. Proust, and J. Lesueur, Phys. Rev. Lett. **108**, 247004 (2012); e-print arXiv:1112.2633v1.
[40]S. Su, J. Ho You, and C. Lee, J. Appl. Phys. **113**, 093709 (2013).
[41]A. F. Santander-Syro, O. Copie, T. Kondo, F. Fortuna, S. Pailhès, R. Weht, X. G. Qiu, F. Bertran, a. Nicolaou, a. Taleb-Ibrahimi *et al.*, Nature **469**, 189 (2011).
[42]R. C. Neville, B. Hoeneisen, and C. A. Mead, J. Appl. Phys. **43**, 2124 (1972).
[43]W.-J. Son, E. Cho, B. Lee, J. Lee, and S. Han, Phys. Rev. B **79**, 245411 (2009).
[44]R. Pentcheva, M. Huijben, K. Otte, W. E. Pickett, J. E. Kleibeuker, J. Huijben, H. Boschker, D. Kockmann, W. Siemons, G. Koster *et al.*, Phys. Rev. Lett. **104**, 166804 (2010).
[45]Z. Zhong, A. Tóth, and K. Held, Phys. Rev. B **87**, 161102(R) (2013).
[46]S. Thiel, G. Hammerl, A. Schmehl, C. W. Schneider, and J. Mannhart, Science **313**, 1942 (2006).
[47]C.-L. Jia, V. Nagarajan, J.-Q. He, L. Houben, T. Zhao, R. Ramesh, K. Urban, and R. Waser, Nat. Mater. **6**, 64 (2007).
[48]J. C. Agar, A. R. Damodaran, G. A. Velarde, S. Pandya, R. V. K. Mangalam, and L. W. Martin, ACS Nano **9**, 7332 (2015).

Reuse of AIP Publishing content is subject to the terms at: https://publishing.aip.org/authors/rights-and-permissions. IP: 144.118.64.216 On: Tue, 01 Mar 2016 11:09:11